ACS NANO
Cite This: ACS Nano 2017, 11, 12087−12093
www.acsnano.org

ARTICLE

Engineering Stability-Tunable DNA Micelles Using Photocontrollable Dissociation of an Intermolecular G-Quadruplex

Cheng Jin,[†] Xiaojing Liu,[†] Huarong Bai,[†] Ruowen Wang,[†,§] Jie Tan,[†] Xuehui Peng,[‡,⊥] and Weihong Tan*[,†,‡,§]

[†]Molecular Science and Biomedicine Laboratory, State Key Laboratory of Chemo/Biosensing and Chemometrics, College of Chemistry and Chemical Engineering, College of Life Sciences, Aptamer Engineering Center of Hunan Province, Hunan University, Changsha, Hunan, 410082, China

[§]Institute of Molecular Medicine, Renji Hospital, Shanghai Jiao Tong University School of Medicine, and College of Chemistry and Chemical Engineering, Shanghai Jiao Tong University, Shanghai, China

[⊥]Key Laboratory of Interfacial Reaction & Sensing Analysis in Universities of Shandong, School of Chemistry and Chemical Engineering, University of Jinan, Jinan, Shandong 250022, People's Republic of China

[‡]Department of Chemistry and Department of Physiology and Functional Genomics, Center for Research at the Bio/Nano Interface, UF Health Cancer Center, UF Genetics Institute, McKnight Brain Institute, University of Florida, Gainesville, Florida 32611-7200, United States

Supporting Information

ABSTRACT: **Because of their facile preparation, small size (<100 nm), programmable design, and biocompatibility, lipid-based DNA micelles show enormous potential as a tool to monitor biological events and treat human diseases. However, their structural stability in biological matrices suffers from spatiotemporal variability, thus limiting their *in vivo* use. Herein, we have engineered stability-tunable DNA micelle flares using photocontrollable dissociation of intermolecular G-quadruplexes, which confers DNA micelle flares with robust structural stability against disruption by serum albumin. However, once exposed to light, the G-quadruplex formation is blocked by strand hybridization, resulting in the loss of stability in the presence of serum albumin and subsequent cellular uptake. This programmable regulation to stabilize lipid-based micelles in the presence of fatty-acid-binding serum albumin should further the development of biocompatible DNA micelles for *in vivo* applications.**

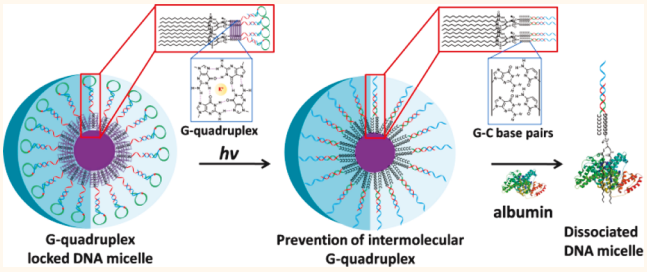

KEYWORDS: *DNA micelles, structural stability, self-assembly, G-quadruplex, photoirradiation*

For biological use, optimal physicochemical properties (*e.g.*, shape, size, stability, and surface groups) of nanoparticles demonstrate spatiotemporal variance within the living body.[1−4] Such variability has stimulated the development of advanced nanoparticles that can change their physicochemical properties in response to internal or external stimuli for improved biocompatibility.[5−7]

Lipid-based DNA micelles are three-dimensional spherical nanoparticles self-assembled from amphiphilic molecules composed of two segments: programmable DNA strands as corona and hydrophobic lipid tails as core. Thus, because of their facile preparation, small size (<100 nm), programmable design of DNA, and biocompatibility, these well-defined nanostructures show enormous potential as a tool to monitor biological events and treat human diseases.[8−10] However, optimum structural stability in biological matrices is subject to spatiotemporal variability, thus limiting the use of DNA micelles, particularly *in vivo*. For example, in blood circulation, DNA micelles need to maintain their structure in order to avoid intrinsic insertion into the hydrophobic core of serum albumin.[11−15] Complexes of lipid-conjugated DNA−serum albumin accumulate at metabolism- or immune-related organs, like the liver[16] and lymph nodes,[17] possibly indicating that these DNA micelles could lose their functionality in other organs. On the other hand, upon reaching their target of interest, micelles must dissociate for effective cellular uptake

Received: July 11, 2017
Accepted: December 12, 2017
Published: December 12, 2017

Downloaded via UNIV OF FLORIDA on July 1, 2018 at 21:53:26 (UTC).
See https://pubs.acs.org/sharingguidelines for options on how to legitimately share published articles.

© 2017 American Chemical Society

DOI: 10.1021/acsnano.7b04882
ACS Nano 2017, 11, 12087−12093

Scheme 1. Schematic of stability-tunable DNA micelles. Intermolecular G-quadruplex stabilizes DNA micelles against disruption by serum albumin. However, upon exposure to UV light, C6-cDNA is released to block the formation of G-quadruplex, resulting in the dissociation of micelles in serum albumin. Note: Purple core inside of micelle indicates hydrophobic lipid core.

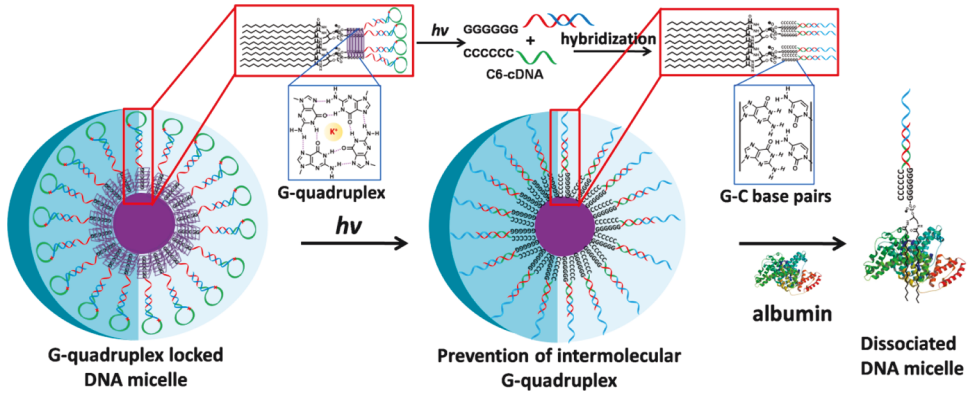

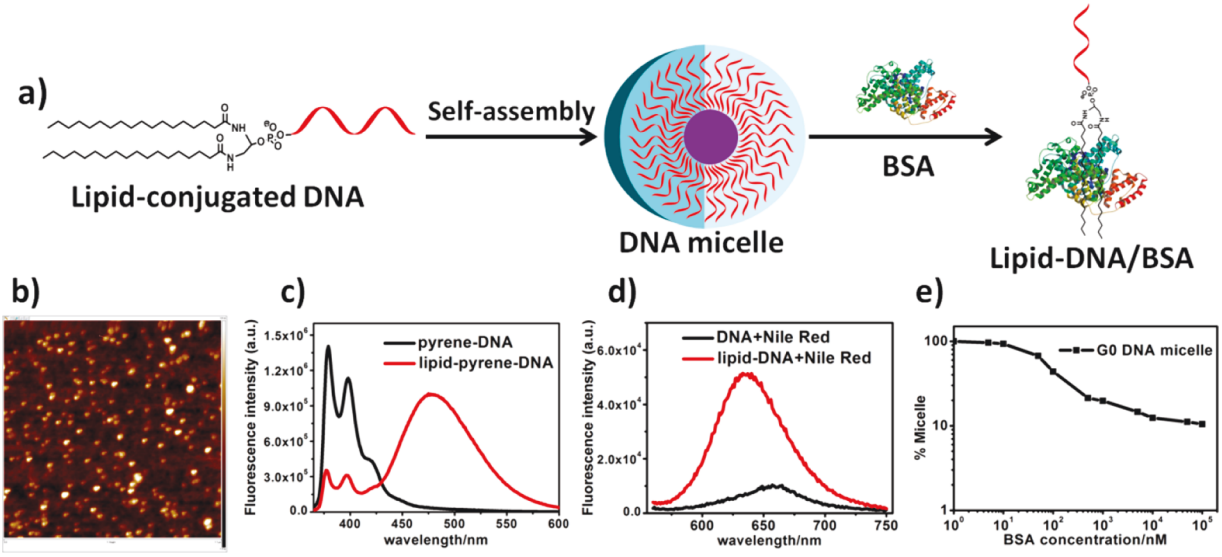

Figure 1. (a) Schematic of self-assembly of DNA micelles and their disruption in the presence of serum albumin (BSA). (b) AFM image of DNA micelle. For lipid-based DNA micelles (28-base DNA), the particle size is about 32 nm. (c) Fluorescence spectroscopy of pyrene-modified DNA and DNA micelles. Emission at 375 and 475 nm indicates monomeric and excimer fluorescence of the pyrene molecule, respectively. (d) Fluorescence spectroscopy of Nile Red dye incubated with lipid-conjugated DNA (red line) and DNA alone (black line). (e) Calculated percentage of DNA micelles in micellar state with the increase of BSA concentration.

and drug delivery. These circumstances call for stability-tunable DNA micelles.

Recently, intermolecular G-quadruplexes[17] and covalent cross-links[18] have been employed as adhesives to stabilize DNA micelles. However, studies reporting stability-tunable DNA micelles are scarce. Therefore, in the present work, we draw on the marked difference in stability between DNA micelles with and without G-quadruplexes and reason that regulated formation of G-quadruplexes can alter the stability of G-quadruplex-locked DNA micelles against the disruption of serum albumin. As a remote control over spatiotemporal response, photoirradiation was chosen as a noninvasive technique in this design. As shown in Scheme 1, before UV irradiation, C6-cDNA (complementary DNA with six cytosine bases at the 3′-terminus to block the formation of G-quadruplex) is caged in the hairpin DNA and cannot block the formation of a G-quadruplex. However, upon exposure to UV light, C6-cDNA is released to hybridize with G6 DNA, thereby blocking the formation of intermolecular G-quadruplexes and resulting in the dissociation of micelles by the bovine serum albumin (BSA) solution. Importantly, after photoirradiation, DNA micelles display robust cellular uptake. This programmable regulation to stabilize lipid-based micelles in the presence of fatty-acid-binding serum albumin should further the development of biocompatible DNA micelles for *in vivo* applications.

RESULTS/DISCUSSION

Lipid-based DNA micelles were formed by hydrophobic self-assembly from lipid-conjugated DNA in DPBS buffer with 5 mM Mg^{2+} (Figure 1a). Atomic force microscopy (AFM) analysis indicates their spherical structure and uniform size (Figures 1b and S7). Pyrene molecules, which have excimer fluorescence in the aggregated state, were also used to prove the formation of the micelle structure.[19] As shown in Figure 1c, a bright excimer fluorescence peak was observed at 475 nm, demonstrating the formation of aggregated micelle particles in lipid-conjugated DNA solution. In contrast, DNA without lipid tail has no emission at 475 nm, indicating the presence of

DOI: 10.1021/acsnano.7b04882
ACS Nano 2017, 11, 12087−12093

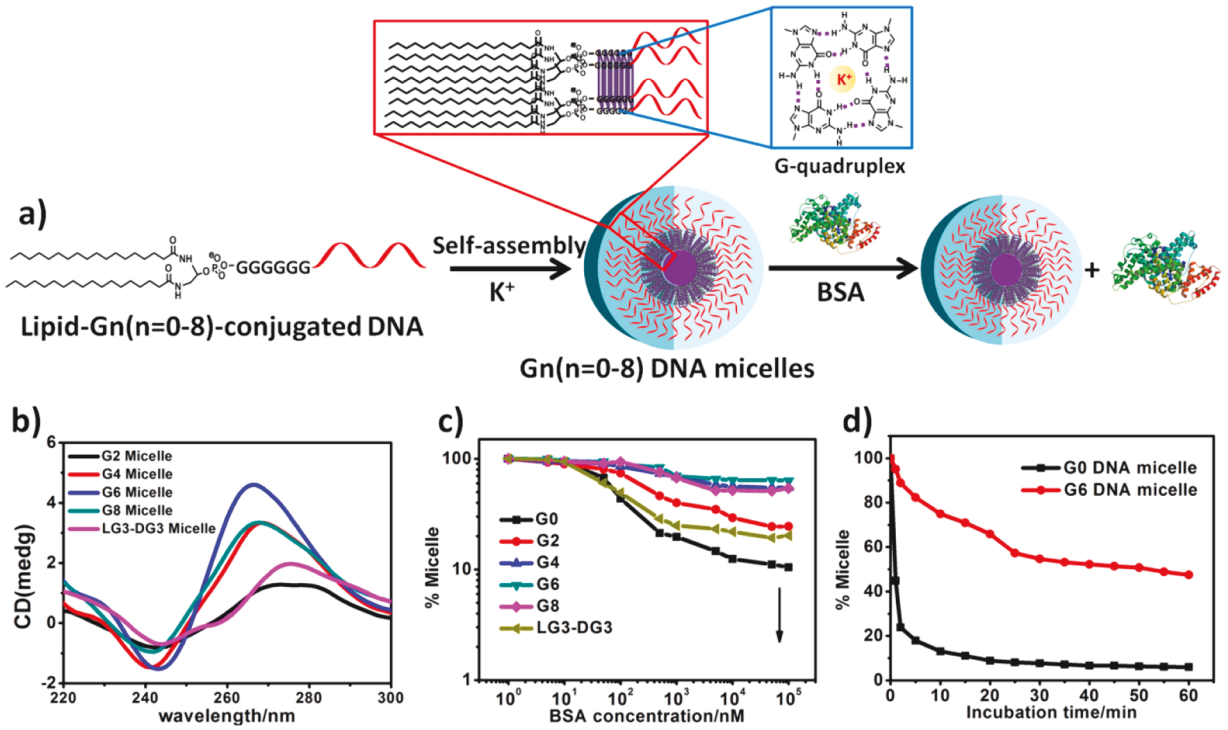

Figure 2. (a) Schematic of self-assembly of G-quadruplex-locked DNA micelles and their stability in BSA solution. (b) CD spectrum of G-quadruplex-locked DNA micelles. The formation of G-quadruplex among DNA strands was indicated by the shifting of positive peaks from 278 nm toward 262 nm and troughs at 245 nm, as the number of guanines in the structure increased. (c) Calculated percentage of DNA micelles with or without G-quadruplex in the presence of BSA for 20 min incubation. (d) Time-dependent analysis of the percentage of G6 DNA micelles and G0 DNA micelles in the presence of 10 μM BSA.

monomeric DNA (Figure 1c, black line). Nile Red, a fluorescent dye that displays significant fluorescence in hydrophobic media, but negligible emission in aqueous solution, was used to determine the encapsulation of guest molecules to further assess the formation of the micellar structure.[20] Nile Red incubated with lipid-conjugated DNA displays a significant fluorescence emission at 635 nm, indicating the formation of a hydrophobic core (Figure 1d). This cumulative evidence supports the self-assembly of lipid-conjugated DNA into micelle nanoparticles.

Having confirmed the formation of DNA micelles from lipid-conjugated DNA, we further investigated the stability of DNA micelles in the presence of serum albumin. It is well-known that serum albumin is a transporter of fatty acids in blood circulation; therefore, the stability of lipid-based DNA micelles in the presence of serum albumin would affect their use, particularly when injected into the body through a vein. Figure 1e shows the calculated percentage of lipid-conjugated DNA in the micellar state after incubation with BSA. About 93% of lipid-conjugated DNA was dissociated into its monomeric state when incubated with 0.1 mM BSA. Since the concentration of serum albumin in blood is about 0.51−0.85 mM, which is greater than 0.1 mM, we can conclude that the injection of native DNA micelles into blood would result in complete dissociation of the micelles by serum albumin.[15]

The complex of monomeric lipid-conjugated DNA−serum albumin accumulates at immune or metabolic organs, such as the liver[16] and lymph nodes.[17] This could indicate that unstable, *i.e.*, dissociated, DNA micelles would most likely not reach their target of interest. Therefore, techniques to stabilize the spherical structure of DNA micelles may improve their utility *in vivo*. Herein, intermolecular parallel G-quadruplexes were introduced into DNA micelles to lock the whole structure, resulting in enhanced stability (Figure 2a). Circular dichroism (CD) analysis of DNA micelles modified with guanine bases demonstrates the formation of parallel G-quadruplexes among lipid-conjugated DNA strands, but only when the number of guanine bases exceeds two (Figure 2b). Additionally, gel electrophoresis analysis of G6 DNA micelles indicates that almost all G6 DNA micelles were locked by G-quadruplexes (Figure S10).

Next, the stability of G-quadruplex-locked DNA micelles in BSA solution was investigated. As shown in Figure 2c, G-quadruplex-locked DNA micelles show significant improvement in structural stability compared to that of micelles without a G-quadruplex. For instance, G6 DNA micelles maintain about 73% micellar structure compared to 7% for G0 (zero guanine bases) DNA micelles. Additionally, time-dependent results of G6 and G0 DNA micelles treated with 10 μM BSA indicate that G0 DNA micelles lost their structures quickly (<10 min), whereas G6 DNA micelles maintained about 50% of their structures, even after one hour (Figure 2d). In the presence of potassium ion, neighboring guanine bases in the micellar corona formed a G-quadruplex *via* Hoogsteen hydrogen bonds and confined the hydrophobic lipid tails inside the micelle core, resulting in stabilization of the micellar structure. LG3-DG3 DNA micelles, which have three guanines in L-chirality and three guanines in D-chirality, were used to assay the effect of chirality of guanine nucleotide on the stability of DNA micelles. In Figure 2c, it can be seen that LG3-DG3 failed to significantly improve the stability of DNA micelles compared to G0 (Figure 2c). This was attributed to the incomplete formation of the G-quadruplex (Figure 2b). Additionally, G-quadruplex-locked

DOI: 10.1021/acsnano.7b04882
ACS Nano 2017, 11, 12087−12093

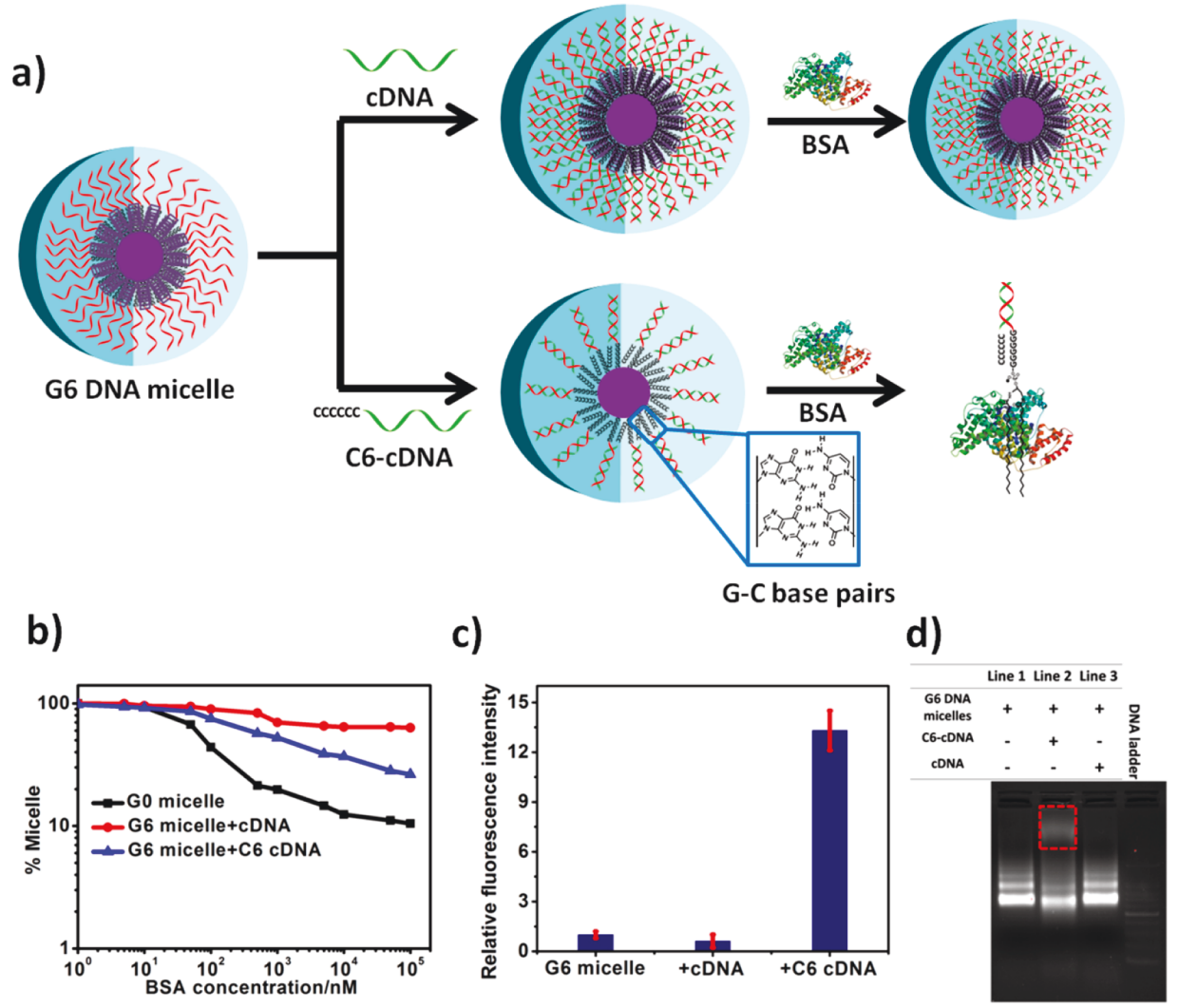

Figure 3. (a) Schematic showing programmable regulation of structural stability for G-quadruplex-locked DNA micelles by strand hybridization. (b) Stability of G6 DNA micelles pretreated with C6-cDNA (blue line) and cDNA (red line) in the presence of BSA. (c) Cellular binding of G6 DNA micelles to CEM cells before and after treatment with cDNA or C6-cDNA, as determined by flow cytometry. Note: Left shows G6 DNA micelles alone; middle shows G6 DNA micelles+cDNA; right shows G6 DNA micelles+C6-cDNA. (d) 2% agarose gel electrophoresis of G6 DNA micelles before and after hybridization with cDNA and C6-cDNA. The tailed DNA band in red indicates unstable DNA micelles. In contrast, G6 DNA micelles alone and hybridization of micelles with cDNA have no tailed DNA band.

DNA micelles displayed excellent stability in cell lysate compared to G0 and LG3-DG3 DNA micelles (Figure S12).

Taken together, this evidence demonstrates that the incorporation of G-quadruplexes into DNA micelles significantly improved their structural stability. However, G6 DNA micelles showed only negligible cellular binding compared to G0 DNA micelles (Figures S13, S14, and S15). This is attributed to the confinement of the hydrophobic lipid tails inside the micelles (Figure S16). Negligible cellular uptake limits intracellular application of G-quadruplex-locked DNA micelles.

The marked difference in stability between G0 and G6 DNA micelles suggested that regulated formation of G-quadruplexes could alter the stability of locked DNA micelles. Based on this principle, C6-cDNA was designed to hybridize with G6 DNA micelles to block G-quadruplex formation. The result indicates that C6-cDNA exerts obvious down-regulation on the stability of G6 DNA micelles (comparison of the percentage of micelles, 21.3% *vs* 71.8%). In contrast, cDNA, without six cytosine bases at the 3′-terminus, has no effect on the formation of G-quadruplexes (67.5% *vs* 71.8%) (Figure 3b). Agarose gel electrophoresis analysis also demonstrates the dissociation of intermolecular G-quadruplexes after hybridization with C6-cDNA, but not with cDNA (Figure 3d). Moreover, after hybridization with C6-cDNA, G6 DNA micelles display obvious cellular binding (about 13-fold) compared to those hybridized with cDNA (Figures 3c and S18).

Generally, it is not easy to find endogenic oligonucleotides with at least four repeated cytosine bases at the 3′-terminus able to hybridize with G-quadruplex-locked DNA micelles in such a narrow space. Therefore, we next looked to other technologies to remotely regulate the release of C6-cDNA. Photocontrollable molecules, such as azobenzene and *o*-nitrobenzyl derivatives, have been widely employed in optogenetics,[21−23] controllable drug delivery[24,25] and nanomotor construction[26−30] because of their noninvasiveness and response to spatiotemporal stimuli. Therefore, a commercially available photocleavable linker (PC linker) was used to cage C6-cDNA in a hairpin DNA (Figure S19). After photoirradiation, C6-cDNA is released and then hybridized with G6 DNA micelles

DOI: 10.1021/acsnano.7b04882
ACS Nano 2017, 11, 12087−12093

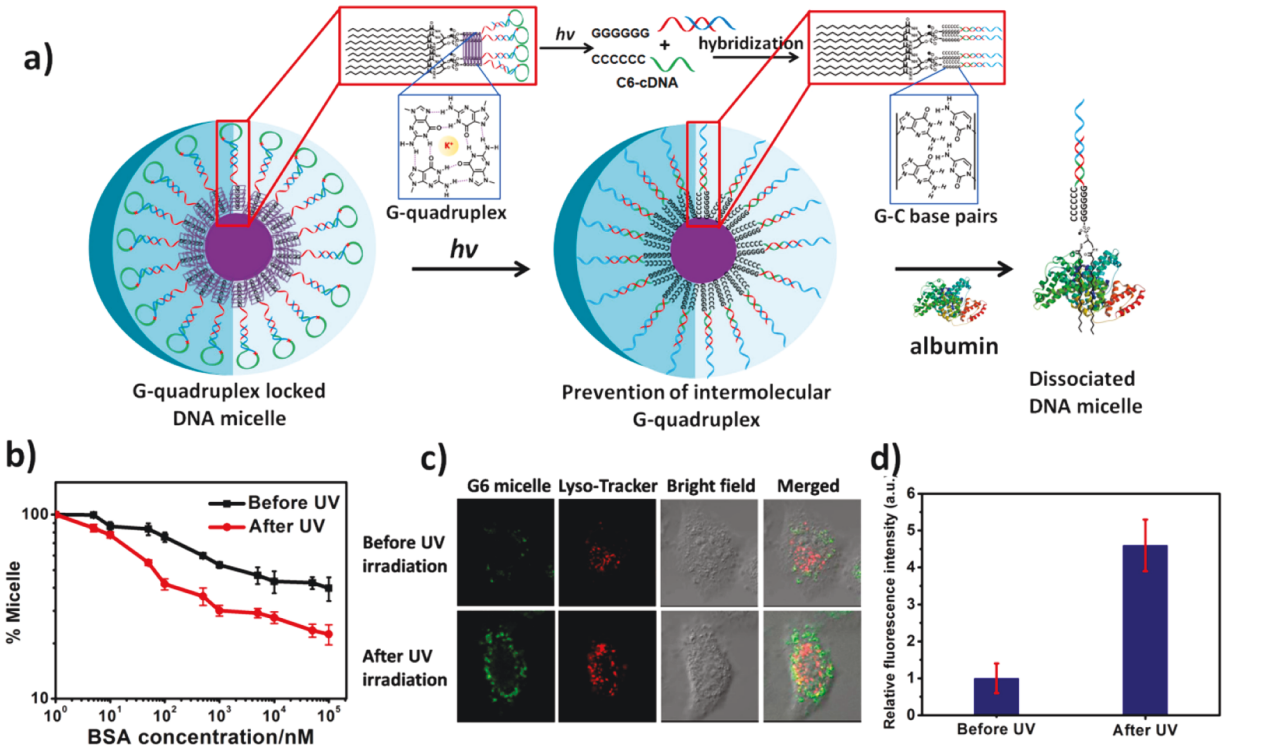

Figure 4. (a) Schematic of G-quadruplex-locked DNA micelles stabilized through photocontrolled regulation. Upon exposure to UV irradiation, C6-cDNA was released to hybridize with G-quadruplex-locked DNA micelles, which resulted in the disruption of DNA micelles in the presence of BSA. (b) Stability of photoregulated DNA micelles before (black line) and after (red line) exposure to light. (c) Confocal fluorescence microscopy imaging of HeLa cells treated with photoregulated DNA micelles before and after UV irradiation. (d) Comparison of relative fluorescence intensity of HeLa cells incubated with photoregulated DNA micelles before and after UV irradiation.

to block intermolecular G-quadruplex formation. This results in the loss of stability of locked DNA micelles in the presence of BSA, leading, in turn, to effective cellular uptake (Figure 4a). Before photoirradiation, about 42.5% of micelles were locked, which is lower than that of G6 DNA micelles (16-base DNA) (73.0%). This can be explained by the higher base number in the photocontrollable G6 DNA micelles system (60 *vs* 16). However, upon exposure to light, obvious loss of stability was observed (21.2% *vs* 42.5%). Gel electrophoresis analysis of this system also indicated partial dissociation of G-quadruplexes after UV irradiation (Figure S20). Importantly, after stimulus, cellular uptake of these micelles by HeLa cells was improved 4.6-fold over these micelles without photoirradiation (Figure 4c and d).

CONCLUSIONS

In summary, hybridization-based molecular engineering was employed to regulate the structural stability of G-quadruplex-locked DNA micelles. Upon exposure to UV light, the G-quadruplex-locked DNA micelles display obvious loss of stability (21.2%) compared to its inert state (42.5%) in the presence of BSA. Importantly, after photoirradiation, photo-regulated DNA micelles now show obvious cellular uptake by about 4.6-fold over that of the inert state, due to unblocking of the hydrophobic lipid tails. This programmable regulation to stabilize lipid-based micelles in the presence of fatty-acid-binding serum albumin should further the development of biocompatible DNA micelles for *in vivo* applications.

METHODS/EXPERIMENTAL

DNA Synthesis. ATGC bases and the labeled phosphoramidite materials used in this article were purchased from Glen Research. Lipid and pyrene phosphoramidite monomers were synthesized in our lab (see details in the Supporting Information). All DNA strands used in this work were synthesized on the PolyGen C12 DNA/RNA solid-phase synthesizer on a 0.1 μM scale, using the corresponding controlled pore glass (CPG). After synthesis, the obtained oligonucleotides were cleaved and deprotected from the CPG, followed by precipitation in cold ethanol solution at −20 °C overnight. After centrifugation to remove the supernatant solution, lipid-conjugated oligonucleotides were dissolved with 0.1 M triethylamine acetate (TEAA) and purified by reversed-phase HPLC using a BioBasic4 column (conventional DNA, C18 reverse-phase HPLC column). Finally, the 4,4′-dimethytribenzyl group was removed from DNA by adding 80% acetic acid aqueous solution and precipitation in cold ethanol again. After drying under vacuum and desalting, the obtained oligonucleotides were quantified by measuring their absorbance at 260 nm.

Preparation of DNA Micelles. DNA micelles with and without G-quadruplex were formed by hydrophobic self-assembly of lipid-conjugated DNA in DPBS solution (5 mM Mg^{2+}). Briefly, the desalted lipid-conjugated oligonucleotides were diluted with DPBS buffer (5 mM Mg^{2+}) to the desired concentration, left at room temperature for about two hours, and then used for the subsequent experiments.

Fluorescence Characterization of Pyrene-Modified DNA Micelles. The fluorescence excimer of pyrene was used to assess the stability of lipid-conjugated DNA micelles against disruption by BSA and cellular lysate. BSA and cellular lysate with the desired concentrations were added to the pyrene-modified DNA micelles solution and incubated for 20 min. Fluorescence spectroscopy was excited at 350 nm, and the emission was collected from 365 to 600 nm with a bandwidth of 5 nm. For time-dependent stability analysis, 10 μM BSA was added to the 1 μM pyrene-modified DNA micelles

DOI: 10.1021/acsnano.7b04882
ACS Nano 2017, 11, 12087−12093

solution and the fluorescence spectra were recorded every five minutes.

Fluorescence Characterization of Nile Red-Encapsulated DNA Micelles. DNA micelles and DNA were diluted with DPBS (5 mM Mg^{2+}) to a final concentration of 1 μM (200 μL), and then 2 μL of Nile Red stock solution (0.1 M in acetone) was added, to give a final Nile Red concentration of 1 μM. The samples were vortexed briefly, sealed, and incubated overnight at room temperature in the absence of light. Fluorescence spectra were recorded at room temperature using an excitation wavelength of 500 nm and monitoring emission between 515 and 750 nm, with excitation and emission slit widths both set at 5 nm.

AFM Analysis of Lipid-Based DNA Micelles. G0 and G6 DNA micelles were diluted to 5 μM in DPBS (5 mM Mg^{2+}) buffer, and 10 μL of this solution was deposited on the freshly cleaved mica surface and allowed to absorb for 5 min. Then 10 μL of Millipore water was dropped on the surface and removed with filter paper. The mica surface was then washed twice with a further 20 μL of Millipore water and dried by nitrogen gas prior to imaging.

Cell Culture. HeLa cells were maintained in DMEM medium supplemented with 10% fetal bovine serum and 0.5 mg/mL penicillin–streptomycin at 37 °C in 5% CO_2. CCRF-CEM (human leukemia) cells were maintained in 1640 medium, supplemented with 10% fetal bovine serum and 0.5 mg/mL penicillin–streptomycin at 37 °C in 5% CO_2.

Cell Lysate Preparation. About two million CCRF-CEM cells were washed twice with DPBS buffer and then dispersed in 500 mL of DPBS buffer solution. The mixture was lysed with a sonicator for 2 min, and the resulting cell lysate solution was used immediately.

Flow Cytometry Analysis. Cells were washed twice with DPBS buffer and then incubated with micelle solution for one hour under 37 °C. After incubation, cells were washed twice with DPBS buffer and then subjected to a FACS assay.

Confocal Fluorescence Microscopy Imaging. HeLa cells were placed in a 35 mm cell culture dish and grown to around 80% confluence for 48 h before the experiment. Cells were washed with 1 mL of DPBS buffer. Then DNA micelles were incubated with cells for the desired time. After incubation, cells were washed twice with DPBS buffer and then subjected to a confocal fluorescence microscopy imaging assay.

Photocontrolled Cleavage of PC Linker. A portable UV lamp (6 W, irradiation at 365 nm) was chosen as light source to cleave the PC linker and thus release C6-cDNA. For controllable cellular uptake, HeLa cells were incubated with micelles and then exposed to a UV lamp for 5 min followed by incubation for an additional two hours. Afterward, HeLa cells with and without photoirradiation were washed twice with DPBS buffer and then subjected to flow cytometry and confocal fluorescence microscopy analysis.

ASSOCIATED CONTENT

Supporting Information

The Supporting Information is available free of charge on the ACS Publications website at DOI: 10.1021/acsnano.7b04882.

NMR characterization of lipid and pyrene phosphoramidite monomers, DNA sequences, HPLC profile and elution program, mass analysis of lipid-conjugated DNA, fluorescence spectroscopy, gel electrophoresis analysis, AFM images, flow cytometry and confocal microscopy images, and illustration of photocaged hairpin DNA structure (PDF)

AUTHOR INFORMATION

Corresponding Author

*E-mail (W. Tan): tan@chem.ufl.edu.

ORCID

Weihong Tan: 0000-0002-8066-1524

Notes

The authors declare no competing financial interest.

ACKNOWLEDGMENTS

This work is supported by NSFC grants (NSFC 21521063 and NSFC 21327009), by NIH GM079359 and NSF 1645215 and also by Key Research and Development Program of Shandong Province, China (No. 2015GGH301001), and the Technology Research Project of Shandong Provincial Education Department (No. J15LC07).

REFERENCES

(1) Cabral, H.; Matsumoto, Y.; Mizuno, K.; Chen, Q.; Murakami, M.; Kimura, M.; Terada, Y.; Kano, M. R.; Miyazono, K.; Uesaka, M.; Nishiyama, N.; Kataoka, K. Accumulation of Sub-100 nm Polymeric Micelles in Poorly Permeable Tumours Depends on Size. *Nat. Nanotechnol.* **2011**, *6*, 815–823.

(2) Petros, R. A.; Desimone, J. M. Strategies in the Design of Nanoparticles for Therapeutic Applications. *Nat. Rev. Drug Discovery* **2010**, *9*, 615–627.

(3) Jiang, W.; Kim, B. Y. S.; Rutka, J. T.; Chan, W. C. W. Nanoparticle-Mediated Cellular Response Is Size-Dependent. *Nat. Nanotechnol.* **2008**, *3*, 145–150.

(4) Ohta, S.; Glancy, D.; Chan, W. C. W. DNA-Controlled Dynamic Colloidal Nanoparticle Systems for Mediating Cellular Interaction. *Science* **2016**, *351*, 841–845.

(5) Wong, C.; Stylianopoulos, T.; Cui, J.; Martin, J.; Chauhan, V. P.; Jiang, W.; Popovic, Z.; Jain, R. K.; Bawendi, M. G.; Fukumura, D. Multistage Nanoparticle Delivery System for Deep Penetration into Tumor Tissue. *Proc. Natl. Acad. Sci. U. S. A.* **2011**, *108*, 2426–2431.

(6) Yoo, J.-W.; Mitragotri, S. Polymer Particles That Switch Shape in Response to a Stimulus. *Proc. Natl. Acad. Sci. U. S. A.* **2010**, *107*, 11205–11210.

(7) Maltzahn, G.; Park, J.-H.; Lin, K. Y.; Singh, N.; Schwoeppe, C.; Mesters, R.; Berdel, W. E.; Ruoslahti, E.; Sailor, M. J.; Bhatia, S. N. Nanoparticles That Communicate *in Vivo* to Amplify Tumour Targeting. *Nat. Mater.* **2011**, *10*, 545–552.

(8) Chen, T.; Wu, C. S.; Jimenez, E.; Zhu, Z.; Dajac, J. G.; You, M.; Han, D.; Zhang, X.; Tan, W. DNA Micelle Flares for Intracellular mRNA Imaging and Gene Therapy. *Angew. Chem., Int. Ed.* **2013**, *52*, 2012–2016.

(9) Wu, C.; Chen, T.; Han, D.; You, M.; Peng, L.; Cansiz, S.; Zhu, G.; Li, C.; Xiong, X.; Jimenez, E.; Yang, C. J.; Tan, W. Engineering of Switchable Aptamer Micelle Flares for Molecular Imaging in Living Cells. *ACS Nano* **2013**, *7*, 5724–5731.

(10) Wu, Y.; Sefah, K.; Liu, H.; Wang, R.; Tan, W. DNA Aptamer-Micelle as an Efficient Detection/Delivery Vehicle toward Cancer Cells. *Proc. Natl. Acad. Sci. U. S. A.* **2010**, *107*, 5–10.

(11) Curry, S.; Mandelkow, H.; Brick, P.; Franks, N. Crystal Structure of Human Serum Albumin Complexed with Fatty Acid Reveals an Asymmetric Distribution of Binding Sites. *Nat. Struct. Biol.* **1998**, *5*, 827–835.

(12) Kratz, F. Albumin as a Drug Carrier: Design of Prodrugs, Drug Conjugates and Nanoparticles. *J. Controlled Release* **2008**, *132*, 171–183.

(13) Spector, A. A. Fatty Acid Binding to Plasma Albumin. *J. Lipid Res.* **1975**, *16*, 165–179.

(14) Wilner, S. E.; Sparks, S. E.; Cowburn, D.; Girvin, M. E.; Levy, M. Controlling Lipid Micelle Stability Using Oligonucleotide Headgroups. *J. Am. Chem. Soc.* **2015**, *137*, 2171–2174.

(15) Lu, J.; Owen, S. C.; Shoichet, M. S. Stability of Self-Assembled Polymeric Micelles in Serum. *Macromolecules* **2011**, *44*, 6002–6008.

(16) Akinc, A.; Zumbuehl, A.; Goldberg, M.; Leshchiner, E. S.; Busini, V.; Hossain, N.; Bacallado, S. A.; Nguyen, D. N.; Fuller, J.; Alvarez, R.; Borodovsky, A.; Borland, T.; Constien, R.; Fougerolles, D. A.; Dorkin, J. R.; Jayaprakash, K. N.; Jayaraman, M.; John, M.; Koteliansky, V.; Manoharan, M.; et al. A Combinatorial Library of

Lipid-Like Materials for Delivery of RNAi Therapeutics. *Nat. Biotechnol.* **2008**, *26*, 561−569.
(17) Liu, H.; Moynihan, K. D.; Zheng, Y.; Szeto, G. L.; Li, A. V.; Huang, B.; Van Egeren, D. S.; Park, C.; Irvine, D. J. Structure-Based Programming of Lymph-Node Targeting in Molecular Vaccines. *Nature* **2014**, *507*, 519−522.
(18) Banga, R. J.; Meckes, B.; Narayan, S. P.; Sprangers, A. J.; Nguyen, S. T.; Mirkin, C. A. Cross-Linked Micellar Spherical Nucleic Acids from Thermoresponsive Templates. *J. Am. Chem. Soc.* **2017**, *139*, 4278−4281.
(19) Liu, H.; Zhu, Z.; Kang, H.; Wu, Y.; Sefan, K.; Tan, W. DNA-Based Micelles: Synthesis, Micellar Properties and Size-Dependent Cell Permeability. *Chem. - Eur. J.* **2010**, *16*, 3791−3797.
(20) Edwardson, T. G. W.; Carneiro, K. M. M.; Serpell, C. J.; Sleiman, H. F. An Efficient and Modular Route to Sequence-Defined Polymers Appended to DNA. *Angew. Chem., Int. Ed.* **2014**, *53*, 4567−4571.
(21) Konermann, S.; Brigham, M. D.; Trevino, A. E.; Hsu, P. D.; Heidenreich, M.; Cong, L.; Platt, R. J.; Scott, D. A.; Church, G. M.; Zhang, F. Optical Control of Mammalian Dndogenous Transcription and Epigenetic states. *Nature* **2013**, *500*, 472−476.
(22) Yizhar, O.; Fenno, L. E.; Davidson, T. J.; Mogri, M.; Deisseroth, K. Optogenetics in Neural Systems. *Neuron* **2011**, *71*, 9−34.
(23) Deisseroth, K. Optogenetics. *Nat. Methods* **2011**, *8*, 26−29.
(24) Liu, J.; Bu, W.; Pan, L.; Shi, J. NIR-Triggered Anticancer Drug Delivery by Upconverting Nanoparticles with Integrated Azobenzene-Modified Mesoporous Silica. *Angew. Chem., Int. Ed.* **2013**, *52*, 4375−4379.
(25) Yuan, Q.; Zhang, Y.; Chen, T.; Lu, D.; Zhao, Z.; Zhang, X.; Li, Z.; Yan, C.-H.; Tan, W. Photon-Manipulated Drug Release from a Mesoporous Nanocontainer Controlled by Azobenzene-Modified Nucleic Acid. *ACS Nano* **2012**, *6*, 6337−6344.
(26) Peng, L.; You, M.; Yuan, Q.; Wu, C.; Han, D.; Chen, Y.; Zhong, Z.; Xue, J.; Tan, W. Macroscopic Volume Change of Dynamic Hydrogels Induced by Reversible DNA Hybridization. *J. Am. Chem. Soc.* **2012**, *134*, 12302−12307.
(27) Beharry, A. A.; Woolley, G. A. Azobenzene Photoswitches for Biomolecules. *Chem. Soc. Rev.* **2011**, *40*, 4422−4437.
(28) Russew, M.-M.; Hecht, S. Photoswitches: from Molecules to Materials. *Adv. Mater.* **2010**, *22*, 3348−3360.
(29) Szymanski, W.; Beierle, J. M.; Kistemaker, H. A. V.; Velema, W. A.; Feringa, B. L. Reversible Photocontrol of Biological Systems by the Incorporation of Molecular Photoswitches. *Chem. Rev.* **2013**, *113*, 6114−6178.
(30) Kang, H.; Liu, H.; Phillips, J. A.; Cao, Z.; Kim, Y.; Chen, Y.; Yang, Z.; Li, J.; Tan, W. Single-DNA Molecule Nanomotor Regulated by Photons. *Nano Lett.* **2009**, *9*, 2690−2696.

DOI: 10.1021/acsnano.7b04882
ACS Nano 2017, 11, 12087−12093